AD-A123 391 CRACK TIP PLASTICITY ASSOCIATED WITH CORROSION ASSISTED FATIGUE(U) SOUTHWEST RESEARCH INST SAN ANTONIO TX D L DAVIDSON ET AL. 31 DEC 82 N00014-75-C-1038 1/1

UNCLASSIFIED F/G 11/6 NL

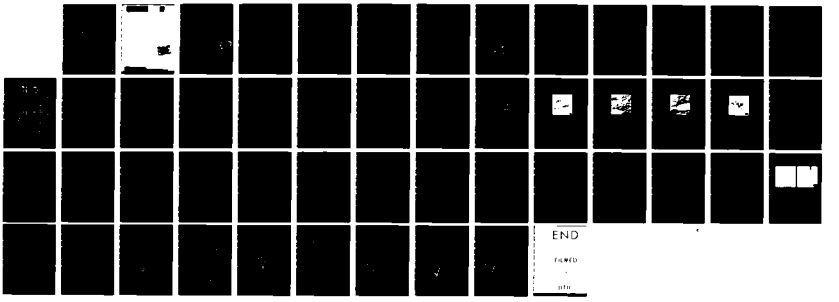

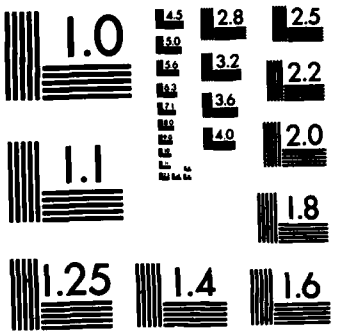

UNCLASSIFIED

SECURITY CLASSIFICATION OF THIS PAGE (When Data Entered)

REPORT DOCUMENTATION PAGE		READ INSTRUCTIONS BEFORE COMPLETING FORM
1. REPORT NUMBER	2. GOVT ACCESSION NO. AD-A123 371	3. RECIPIENT'S CATALOG NUMBER
4. TITLE (and Subtitle) CRACK TIP PLASTICITY ASSOCIATED WITH CORROSION ASSISTED FATIGUE		5. TYPE OF REPORT & PERIOD COVERED FINAL REPORT June 1974-December 1982
	SWRI	6. PERFORMING ORG. REPORT NUMBER ~~06-4268~~
7. AUTHOR(s) D. L. Davidson J. Lankford		8. CONTRACT OR GRANT NUMBER(s) N00014-75-C-1038
9. PERFORMING ORGANIZATION NAME AND ADDRESS Southwest Research Institute 6220 Culebra Road, P.O. Drawer 28510 San Antonio, TX 78284		10. PROGRAM ELEMENT, PROJECT, TASK AREA & WORK UNIT NUMBERS NR 036-109/2-25/76(471)
11. CONTROLLING OFFICE NAME AND ADDRESS Office of Naval Research 800 North Quincy Street Arlington, VA 22217		12. REPORT DATE 31 December 30, 1982
		13. NUMBER OF PAGES 45 + prelims.
14. MONITORING AGENCY NAME & ADDRESS(if different from Controlling Office)		15. SECURITY CLASS. (of this report)
		15a. DECLASSIFICATION/DOWNGRADING SCHEDULE

16. DISTRIBUTION STATEMENT (of this Report)

Reproduction in whole or in part is permitted for any purpose of the United States Government. Distribution is unlimited.

17. DISTRIBUTION STATEMENT (of the abstract entered in Block 20, if different from Report)

18. SUPPLEMENTARY NOTES

19. KEY WORDS (Continue on reverse side if necessary and identify by block number)

Corrosion fatigue	Crack tip strains	Electron channeling
Crack tip plasticity	Aluminum alloys	Subcell
Fatigue-environment interaction	Crack opening displacement	Crack tip stress
Fractography	Low-carbon steel	
Fatigue crack propagation	Stereoimaging	

20. ABSTRACT (Continue on reverse side if necessary and identify by block number)

Measurement of the influence of water vapor in the environment on fatigue crack tip strains and stresses has been the objective of this program. In low-carbon steel, stresses in the plastic zone were deduced by imaging subcells formed during fatigue crack growth. Water vapor was found to lower the stress levels and decrease the size of the zone of stresses exceeding the yield value. Strains within the plastic zone and at the crack tip may be determined by the stereoimaging technique. For low-carbon steel, water vapor lowers the strains carried by the crack tip, and stresses computed from these strains agree well

DD FORM JAN 73 1473 EDITION OF 1 NOV 65 IS OBSOLETE

UNCLASSIFIED

SECURITY CLASSIFICATION OF THIS PAGE (When Data Entered)

with those determined from measurement of subcell size. A manuscript is included in this report which describes the computational technique of converting strains to stresses.

Strains in the crack tip region have been extensively determined for aluminum alloys: 7075-T651 ingot alloy and an experimental powder metallurgy alloy MA-87. Water vapor in the environment is shown to have a similar effect on strains as in low-carbon steel. Dynamic observations of crack growth in vacuum have revealed that cracks do not grow on each cycle. Fractography supports both of these observations, and reveals many other details of crack growth as well.

Detailed crack tip measurements have revealed the fact that crack opening is mixed mode even though loading is purely Mode I. The degree of Mode II in the crack opening is strongly influenced by the environment, level of cyclic stress intensity factor, and the metallurgical state of the materials. This finding is potentially a very important outcome of this research.

A significant effort was expended to utilize the factors measured in models for crack growth, and some progress was made.

TABLE OF CONTENTS

SCOPE AND PURPOSE OF INVESTIGATION

Fatigue crack growth has been shown to be dependent on environment, especially at values of cyclic stress intensity factor (ΔK) approaching the threshold value.[(I)*] This behavior has been termed "environmentally-assisted fatigue crack growth"[(II)] to separate this behavior from that related to cyclic stress corrosion. This program was planned to utilize new tools for measuring the effect of environment on the material response (plasticity) associated with fatigue crack growth.

Measurements were made on the effect of environment and ΔK on crack tip plasticity parameters for low carbon steel,[(A,B,C,D,1,2,3)] 7075-T6 ingot aluminum alloy,[(F,G,10,13,17)] MA-87 a powder metallurgy derived aluminum alloy,[(F,G,11,13,16,17)] and Ti-6Al-4V in the recrystallized-annealed condition.[(14)]

Three environments were used: very dry nitrogen (less than 10 ppm water vapor), vacuum of 10^{-5} torr (1.3 mPa) and humid air (not less than 12,000 ppm water vapor). Differences between vacuum and very dry nitrogen results could not be detected.

Two techniques were used to study crack tip plasticity. At the start of the investigation, low-carbon steel was found to form subcells near fatigue cracks,[(A,B,1,2)] and these were readily observed by electron channeling contrast in the SEM.[(19,20)] This technique was used to characterize the subcell distribution as a function of environment and ΔK, and the information was used to derive both the stress distribution near the crack tip, and to compute the energy dissipated during crack growth.[(B,C,5,6,7,8)] Towards the end of this part of the investigation, two new techniques were developed for studying fatigue cracks: a cyclic loading stage was developed for the SEM[(III)] so that high-resolution, real-time observations of crack growth could be made, and the stereoimaging technique[(IV)] was developed for accurate, high-resolution determination of crack tip strains and opening displacements. These new techniques were then applied to all the materials investigated.

---

*A-G refer to technical reports; journal references reporting work from this contract are numbered 1-21; Roman numerals are used to designate journal references not specifically related to this contract.

SUMMARY OF RESULTS

The general finding of this investigation common to all the materials studied is that water vapor in the environment decreases the strain range which the crack tip can support,[7,10,11,14] although for the titanium alloy, this finding is subject to interpretation. A typical result for 7075-T651 is shown in Fig. 1. Crack tip strain and crack opening are found to be strongly dependent on ΔK for both environments and all materials. For near-threshold ΔK, crack tip strain approaches the elastic limit in the absence of water vapor, and there is some evidence, although not conclusive, that crack growth may occur at strains below the elastic limit in the water vapor environment. Again, Ti-6Al-4V does not completely fit this pattern. Another important finding of this research is that cracks do not grow on each cycle in the near-threshold region,[10,11] although in humid air, growth occurs more frequently, i.e., after fewer number of cycles, than in the absence of water vapor.

Crack opening has been found to be mixed mode in each alloy system investigated and under all conditions of stress intensity and environment.[17] But the magnitude of each mode is strongly influenced by each of these variables. Models of crack tip plasticity and opening do not presently consider Mode II (shear) as being a significant factor, yet in MA-87 this is the dominant opening mode.[17] The influence of metallurgical structure on this aspect of crack tip mechanics is potentially an important factor in controlling fatigue crack growth, and needs to be further explored.

The energy dissipated during fatigue crack growth was computed for low carbon steel[B,C,5,6,7,8] and found to depend on environment and stress intensity. These observations and computations were incorporated into a model for near-threshold crack growth.[8] Water vapor in the environment results in a lower rate of energy dissipation per unit of crack formation.

Models for crack growth in the aluminum and titanium alloys have been developed[G,10,11,14] using information determined by the stereo-imaging technique.

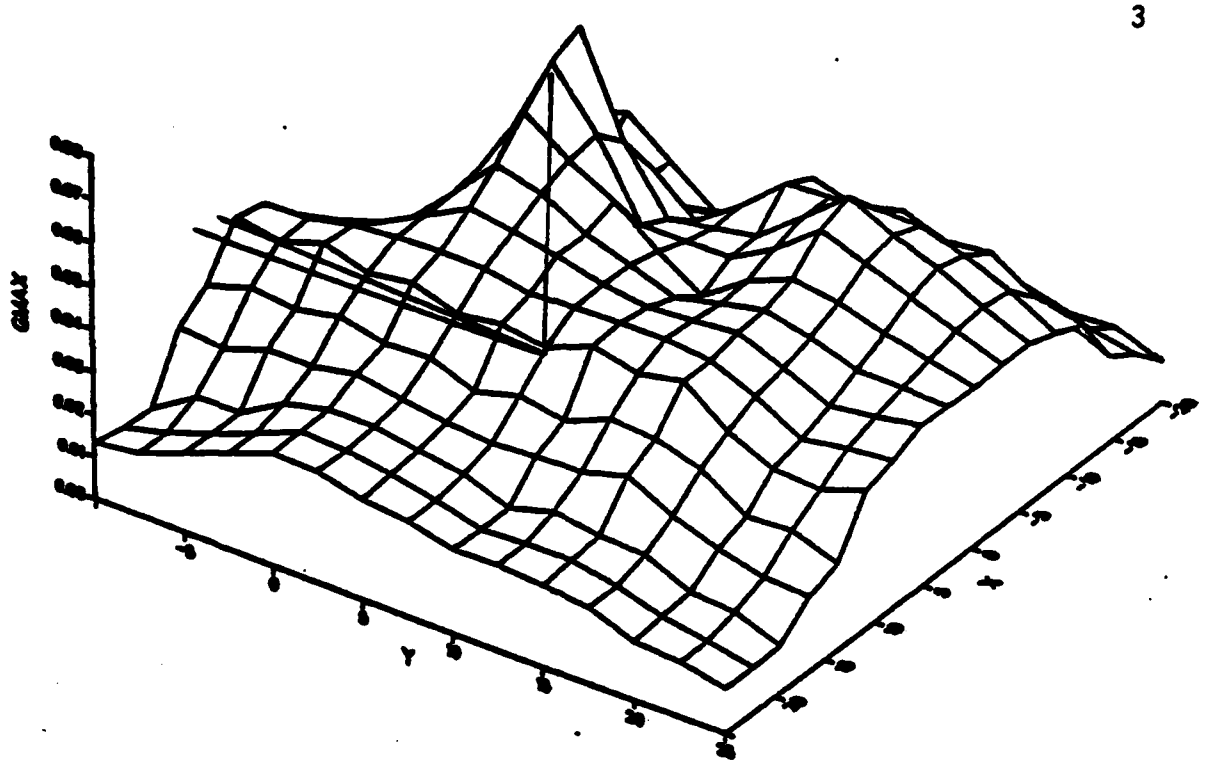

Dry Environment

$\Delta K = 6\ MN/m^{3/2}$

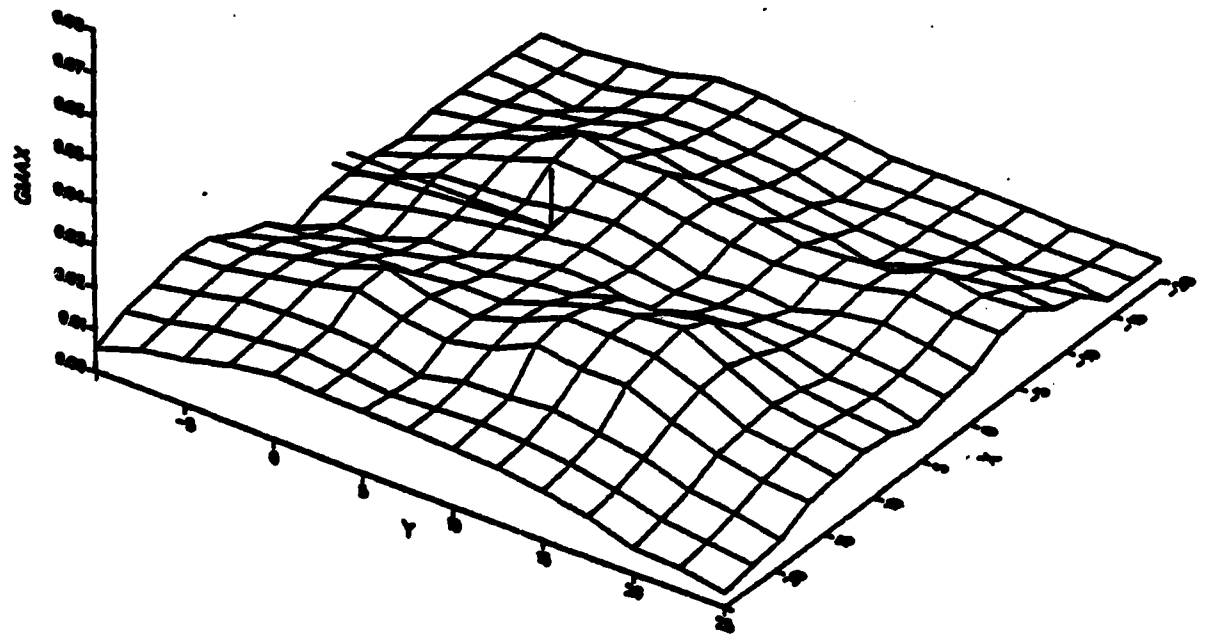

Wet Environment

Figure 1. Distribution of maximum shear strain range for 7075-T651 in both wet and dry environments at $\Delta K = 6\ MN/m^{3/2}$. Crack is shown on the plane of zero strain. X and y are in micrometers. Scale on strain axis is the same for both plots. Water vapor in the environment causes a reduction in the strain range.

The results discussed above are only the most general conclusions reached; there were numerous interesting experimental findings related to both fatigue crack growth, the effect of environment, and the mathematical modeling of fatigue crack growth. These results have been published in the form of annual technical reports and papers. The technical reports have also been used to disseminate more detailed experimental results than it has been possible to put into journal articles. The published papers are more complete and interpretive than the reports. Between these two forms of communication, nearly all the results derived during this research have been reported.

PROJECT SUMMARY

Two new techniques for the study of environmental alteration of material plasticity at crack tips have been developed during the life of this contract. These techniques allow the determination of material stresses and strains within a very small region close to the crack tip (1-10 μm). These measurement techniques were used to determine the effect of environment on fatigue crack growth in low carbon steel, the aluminum alloys 7075-T651 and MA-87 (a P/M product) and Ti-6Al-4V (RA). The information gained by these measurements was used in models whose objectives were to both correlate the various parameters measured and to gain more fundamental insight into the factors controlling environmentally-assisted fatigue crack growth.

CONCLUSIONS

The strain which a crack tip can support is lowered when the crack is grown in a water vapor environment, as compared to a very dry or vacuum environment. Hydrogen formed by dissociation of water vapor at the newly formed surface[V] is believed to cause this "embrittlement." All indications are that the hydrogen is acting within 10 μm of the crack tip, or

less. In aluminum alloys, the details of this effect are influenced by heat treatment and microstructure.

REFERENCES

I. R. O. Ritchie, International Metallurgical Reviews 20, 205 (1979).

II. A. J. McEvily and R. P. Wei, Corrosion Fatigue: NACE 2 Nat. Assoc. of Corrosion Enggrs., Houston, 1972, p. 381-393.

III. D. L. Davidson and A. Nagy, J. Phys. E. 11, 207-210 (1978).

IV. D. R. Williams, D. L. Davidson and J. Lankford, Experimental Mechanics 20, 134-139 (1980).

V. R. P. Wei, P. S. Pao, R. G. Hart, T. W. Weir and G. W. Simmons, Met. Trans. A, 11A, 151-158 (1980).

INDEX OF TECHNICAL REPORTS

Contract N00014-75-C-1038
"Crack Tip Plasticity Associated with Corrosion Assisted Fatigue"

Number	Year	Inclusive Dates	What Reported
A	First	June 1975-June 1976	Measurements on low carbon steel and 6061-T6 aluminum alloy
B	Second	June 1976-June 1977	Extensive measurement on low carbon steel. Computation of energy dissipation during crack growth
C	Third	June 1977-June 1978	Further work on low carbon steel; determination of crack tip stresses from dislocation subcells
D	Fourth	June 1978-June 1979	Direct measurements of crack tip strains using stereoimaging
E	Fifth	June 1979-June 1980	Computation of stress in low carbon steel from stereoimaging strains; comparison of results with those derived from subcells
F	Sixth	June 1980-June 1981	Crack tip openings and strains in 7075-T6 by stereoimaging
G	Seventh	June 1981-September 1982	Crack tip plasticity and crack opening displacements in MA-87 and 7075-T6; detailed fractography of both alloys, and models for fatigue crack growth as a function of stress intensity and environment

INDEX OF PUBLICATIONS

1. "Fatigue Crack Tip Plastic Zones in Low Carbon Steel," by D. L. Davidson, J. Lankford, T. Yokobori, and K. Sato, International Journal of Fracture, Vol. 12, No. 4, p. 579, 1976.

2. "Environmental Alteration of Crack Tip Dislocation Cell Structure and Modes of Growth During Fatigue Crack Propagation in Ferritic Steel," by J. Lankford and D. L. Davidson, International Journal of Fracture, Vol. 12, Reports of Current Research, pp. 775-776, 1976.

3. "The Influence of Water Vapor on Fatigue Crack Plasticity ow Carbon Steel," by D. L. Davidson and J. Lankford, Fourth International Conference on Fracture, Vol. 2, Waterloo, Ca pp. 897-904, 1977.

4. "Nondestructive, Near-Surface Plasticity Determination by Electron Channeling," by D. L. Davidson, Surface Effects in Crystal Plasticity, NATO Advanced Study Institute Series E, edited by R. M. Latanision and J. T. Fourie, Noordhoff International Publishing, pp. 801-809, 1977.

5. "Determination of the Energy of Fatigue Crack Propagation and Alteration by Wet Air," by D. L. Davidson and J. Lankford, Proceedings of the Symposium: Environment Sensitive Fracture of Engineering Materials, edited by Z. A. Foroulis, AIME, pp. 581-594, 1979.

6. "Comparison of Plastic Work of Fatigue Crack Propagation in Low-Carbon Steel Measured by Strain Gages and Electron Channeling," by P. K. Liaw, M. E. Fine, and D. L. Davidson, Fatigue of Engineering Materials and Structures, Vol. 3, pp. 59-74, 1980.

7. "The Effect of Water Vapor on Fatigue Crack Tip Stress and Strain Range Distributions and the Energy Required for Crack Propagation in Low-Carbon Steel," by D. L. Davidson and J. Lankford, International Journal of Fracture, Vol. 17, No. 3, pp. 257-275, 1981.

8. "Incorporating Threshold and Environmental Effects into the Damage Accumulation Model for Fatigue Crack Growth," by D. L. Davidson, Fatigue of Engineering Materials and Structures, Vol. 3, pp. 229-236, 1981.

9. "Crack Tip Stresses as Computed from Strains Determined by Stereoimaging," by D. L. Davidson, D. R. Williams, and J. Buckingham, submitted to Experimental Mechanics.

10. "The Effect of Water Vapor on Fatigue Crack Tip Mechanics in 7075-T651 Aluminum Alloy," by D. L. Davidson and J. Lankford, Fatigue of Engineering Materials and Structures (submitted).

11. "Fatigue Crack Tip Mechanics of a Powder Metallurgy Aluminum Alloy in Vacuum and Humid Air," by D. L. Davidson and J. Lankford, Fatigue of Engineering Materials and Structures (submitted).

12. "The Effect of Metallurgical Structure, Environment and Stress Intensity on Fatigue Crack Tip Plasticity in Al-Zn-Mg-Cu Alloys," by D. L. Davidson and J. Lankford, Fatigue of Engineering Materials and Structures (submitted).

13. "Fatigue Crack Micromechanisms in Ingot and Powder Metallurgy 7XXX Aluminum Alloys in Air and Vacuum," by J. Lankford and D. L. Davidson, Acta Metallurgica (submitted).

14. "Fatigue Crack Growth Mechanics for Ti-6Al-4V (RA) in Vacuum and Humid Air," by D. L. Davidson and J. Lankford, Metallurgical Transactions (in preparation).

15. "A Comparative Analysis of the Effect of Water Vapor on the Crack Tip Plasticity of Steel, Aluminum and Titanium Alloys," by D. L. Davidson and J. Lankford (in preparation).

16. "Fracture Surface Contact and Spherical Debris During Nominal Mode I Fatigue Crack Growth," by J. Lankford and D. L. Davidson, Metallurgical Transactions (submitted).

17. "Mixed Mode Crack Opening in Fatigue," by D. L. Davidson and J. Lankford, Scripta Metallurgica (submitted).

18. "Rotation Between SEM Micrograph and Electron Channeling Patterns," by D. L. Davidson, Journal of Physics E, Vol. 9, p. 341, 1976.

19. "The Use of Channeling Contrast in the Study of Material Deformation," by D. L. Davidson, Scanning Electron Microscopy/1977, Vol. I, IIT Research Institute, pp. 431-438, 1977.

20. "The Use of Subgrains as Imaged in the SEM from Bulk Specimens in the Study of Localized Plasticity," by D. L. Davidson, Scanning, Vol. 2, pp. 225-229, 1979.

21. "Backscattered Electrons in the SEM: Techniques and Uses in Metallurgy," by D. L. Davidson, Microbeam Analysis-1981, R. Geiss, ed., San Francisco Press, pp. 17-23, 1981.

[illegible] OF MODE II CRACKING OF MODE I [illegible] IN AN ALUMINUM ALLOY

[illegible] and D. L. Davidson
Department of Materials Sciences
Southwest Research Institute
San Antonio, Texas 78228

Recently, the authors utilized a new high resolution displacement measuring technique, involving the analysis of stereomicrographs[1] of the tips of fatigue cracks loaded within the SEM,[2] to show that cracks subject to nominal Mode I loading actually open in a way Modes I and II. This effect was observed to be much more pronounced in a powder metallurgy alloy[3] than in an equivalent (composition and mechanical properties) ingot metallurgy material.[4] The purpose here is to report the surprising fractographic observations associated with this change in crack opening mode.

In the studies referenced above,[3,4] the [illegible] of powder metallurgy PM-87 (Al-8Fe-4Ce) and ingot metallurgy 7075-T651 aluminum alloys were tested in air and vacuum over the cyclic stress intensity range $6 \leq \Delta K \leq 12$ MNm$^{-3/2}$ at R = 0.1. Stereoimaging[1] was used to determine the crack tip opening displacement (Figure 1) and crack opening mode behind the tips of long, Mode I-loaded cracks; representative results extrapolated to 1 μm behind the tip, for $\Delta K = 7.5$ MNm$^{-3/2}$, are summarized in Table I. From the table, it is clear that in 7075-T651, Mode I crack opening predominates, as expected, in both air and vacuum, while for the powder metallurgy alloy, crack tip opening displacement (CTOD) is achieved primarily through Mode II. Furthermore, the CTOD in PM-87 exceeds that of 7075-T651 by a factor of about 3.5 times.

TABLE I

CRACK TIP OPENING PARAMETERS 1 μm BEHIND CRACK TIP,
$\Delta K = 7.5\ MNm^{-3/2}$

Alloy	Environment	$CTOD_I$ (μm)	$CTOD_{II}$ (μm)	CTOD* (μm)	$CTOD_{II}/CTOD_I$
7075-T6	Air	0.238	.077	0.25	.32
7075-T6	Vacuum	0.17	.10	0.20	.59
MA-87	Air	0.47	.77	0.90	1.64
MA-87	Vacuum	0.54	.72	0.90	1.33

*$CTOD = \sqrt{CTOD_I^2 + CTOD_{II}^2}$

The fractography of 7075-T651 is conventional over this stress intensity regime, i.e., striations are formed in both air and vacuum.[5] The behavior of MA-87 is markedly different. In vacuum, for example, fatigue crack growth produces approximately spherical particles, which are dispersed over a fractographic background of diffuse, ripply striations; these features are observed uniformly across the specimen fracture surface. The particles usually are observed as isolated individuals, but they frequently occur in clusters (Figures 2 and 3) as well. Energy dispersive X-ray analysis (EDS) of several of the spheres showed that they have the same chemical makeup as the matrix material. Thus, the spheres do not correspond to the small (0.02 μm to 0.3 μm) Co_2Al_9 dispersoid particles[6]

characteristic of MA-87. However, it is possible to derive some idea as to their origin by considering clusters of the spheres in various stages of development.

For example, in Figure 2 can be seen a large, smooth platelet (P), from which several connected spheres (A) have separated. Since it appears that the platelet and the spheres once fit together, the spheres evidently formed while still attached to the platelet. Other spheres, such as B, show what appear to be laps, as though they had been flattened out and then rolled up. Once a platelet is formed, parts of it evidently begin to roll up; these eventually detach from the parent platelet by fracture, to form separate spheres such as C in Figure 3. Note the apparent rolled-up pre-sphere on platelet P in this figure.

It would appear that the critical step in sphere formation is the creation of the platelets. Such features have in fact been observed before, but only in cases in which Mode II interfacial sliding was externally imposed by the specific loading conditions. These have included fretting fatigue,[7] rolling contact,[8] and pure Mode II fatigue,[9] i.e., cyclic compression of slant cracks. Under such circumstances, localized regions of opposing surfaces experience sliding contact, each producing an extraordinarily smooth, thin layer of material known as a Beilby layer.[10] The Beilby layer has the same chemical composition as the parent alloy, but crystalline order is almost destroyed by the rubbing process, and the end product is extremely ductile. It is this anomalous ductility which permits the layers to roll up into laminated spheres.[10]

It is interesting that spheroidal debris is not found on MA-87 fatigue fractures formed in air. Instead, the surface is heavily oxidized (Figure 4), so much so that striations, although present, are hard to discern. Superimposed on the fracture surface are very small, round particles, seemingly embedded in the fracture surface. These are much smaller than the spherical wear particles formed in vacuum, and are of the size, shape, and spacing of the Co_2Al_9 dispersoids. Electron beam diameter and penetration into the underlying substrate preclude EDS determination of their composition.

Irregular-shaped bits of apparent oxide debris (arrow, Figure 4) also are evident. Their presence is best appreciated by examining the flanks of cracks grown in air; these are seen to exude debris (Figure 5). The electron-charging nature of the debris strongly suggests that it derives from fractured oxide films.

By considering certain recent, related research involving similar alloys, it is possible to understand the tendency of MA-87, but not 7075-T651, to produce wear debris, and for the MA-87 debris particles to be smooth and spherical in vacuum, while rough and irregular in air. In the first case, Vasudevan and Suresh[11] have recently investigated the oxide-forming propensity of 7XXX aluminum alloys, of which MA-87 is a variant. Among their findings is the fact that during fatigue crack growth in air, the level of oxide formation on fresh crack surface is on the order of 0.01 μm, negligible compared to crack tip opening displacements (Table I), for peak-aged alloys like 7075-T651. However, for overaged alloys like

MA-87*, oxide layers of up to 0.1 μm in thickness are produced during fatigue crack growth in moist air at near-threshold stress intensities.

Rabinowicz[12] has noted that oxidation during sliding contact will generally lead to the formation of debris which prevents two-body burnishing. The debris occurs by the fracture and spalling-off of the oxide layer. In the present case, this process apparently accounts for the debris which is extruded during the growth of cracks in MA-87 in air; it will be recalled (Table I) that the Mode II crack tip displacement component is quite large relative to the total CTOD. For 7075-T651, the oxide layer formed in air is negligible, and so is the Mode II opening displacement; hence, no oxide debris is observed.

On the other hand, there is no oxide layer to prevent the local burnishing of MA-87 crack interfaces in vacuum, and together with the large Mode II crack tip displacement, the formation of Beilby layers and their transformation to spheroidal debris is favored. Although there is also no oxide to prevent burnishing of 7075-T651 in vacuum, the Mode II displacement in this case is insufficient to produce the requisite damage layers. Comparing the $CTOD_{II}$ values for 7075-T651 and MA-87 in vacuum (Table I), it appears that the threshold Mode II displacement for the production of spherical wear particles in 7XXX aluminum alloys must lie between 0.1 μm and 0.72 μm. It also is interesting to note that the largest MA-87 spheroidal particles are on the same order of size as $CTOD_{II}$.

---

*Heat treatment was -T6 plus 14 hours at 162C.

If these rationalizations are correct, then it must also be true that the crack faces do not open in Mode I before at least some sliding has occurred. To verify this, the opening of MA-87 crack tips was photographed at various increments in the load cycle, and the resulting micrographs were analyzed using stereoimaging. It was found that as the cyclic stress increases from its minimum value, the crack tip starts sliding at a very low stress intensity; Mode I opening is not achieved until $\Delta K \simeq 0.5\ K_{max}$. Thus, there is ample opportunity for interfacial contact during Mode II sliding.

At present, it is not at all clear <u>why</u> fatigue cracks in MA-87 choose to open in mixed Modes I and II, while 7075-T651 cracks open predominantly in Mode I; neither is it apparent why the CTOD for MA-87 is so much greater than that for 7075-T651. Aside from grain size, ~50 μm for 7075-T651 versus ~5 μm for MA-87, the principal differences between the two alloys lie in their microstructures. MA-87 is overaged, and has a low dispersoid population, while 7075-T651 is peak-aged, with a high dispersoid content.

Regardless of the origin of the Mode II opening in MA-87, its presence is remarkable, considering the relatively low driving force responsible for it. Analysis of the present crack profiles shows that on average, for both alloys in air and vacuum, a given crack segment is oriented approximately 25° from normal to the stress axis. Under such circumstances,[13] the Mode I stress intensity normal to the local crack plane is .82 of the Mode I stress intensity (K_I) for the average crack plane. Correspondingly, the local Mode II stress intensity is only .38 K_I.

The presence of the wear debris itself has implications for fatigue crack growth, since Vasudevan and Suresh[11] have shown that the presence of oxide layers alone can significantly alter the effective Mode I stress intensity at low rates of growth. The existence of the oxide wear debris (Figure 5) means that the wedging effect of the oxide layer is further enhanced in materials which have a large Mode II crack opening component, since the fracturing of the oxide layers will promote the formation of new oxide, effectively increasing the thickness of the layer. Similarly, the presence of the spherical debris in vacuum corresponds to a wedging influence which will likewise tend to reduce the Mode I effective stress intensity.

These conclusions are supported by the work of Ryder, et al,[14] who studied the behavior of torsional Stage I cracks in an Al-Mg-Zn alloy. They found that Stage I (Mode II) crack growth rates were enhanced by inert liquids which normally retard Stage II (Mode I) crack growth. The effect of the liquids was to pump out of the crack fretting debris produced by Mode II sliding, thereby increasing the effective stress intensity.

Acknowledgement

The authors are grateful for the support of the Office of Naval Research through Contract No. N00014-75-C-1038.

References

1. D. R. Williams, D. L. Davidson, and J. Lankford, Exp. Mech., 1980, Vol. 20, p. 134.
2. D. L. Davidson and A. Nagy, J. Phys. E, 1978, Vol. 11, p. 207.
3. D. L. Davidson and J. Lankford, Fat. Eng. Mat. Struct. (submitted).
4. Ibid.
5. J. Lankford and D. L. Davidson, Acta Metallurgica (submitted).
6. S. H. Doerr, "A Comparison of Microstructure and Properties of Equivalent Strength Ingot Metallurgy and Powder Metallurgy 7XXX Aluminum Alloys," AFWAL-TR-81-4068, 1981.
7. P. H. Hurricks, Wear, 1974, Vol. 27, p. 319.
8. D. Scott and G. H. Mills, Wear, 1973, Vol. 24, p. 235.
9. M. C. Smith and R. A. Smith, Wear, 1982, Vol. 76, p. 105.
10. D. Scott, W. W. Seifert, and V. C. Westcott, Sci. Amer., 1974, Vol. 230, p. 88.
11. A. K. Vasudevan and S. Suresh, Met. Trans. A (in press).
12. E. Rabinowicz, Wear, 1977, Vol. 42, p. 149.
13. A. B. Patel and R. K. Pandey, Fat. Eng. Mat. Struct., 1981, Vol. 4, p. 65.
14. D. A. Ryder, M. Martin, and M. Abdullah, Met. Sci., 1977, Vol. 11, p. 340.

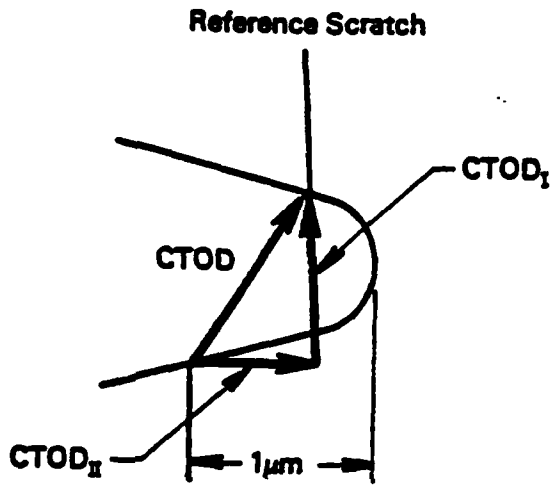

Figure 1. Schematic of crack tip opening parameters, showing displacement of a hypothetical reference mark 1 μm behind the crack tip.

Figure 2. Spheroidal wear debris on fatigue fracture surface of MA-87, vacuum environment, $\Delta K = 7\ MNm^{-3/2}$. Platelet (P), separated spheroids (A), lapped spheroid (B). Large arrow shows direction of crack growth.

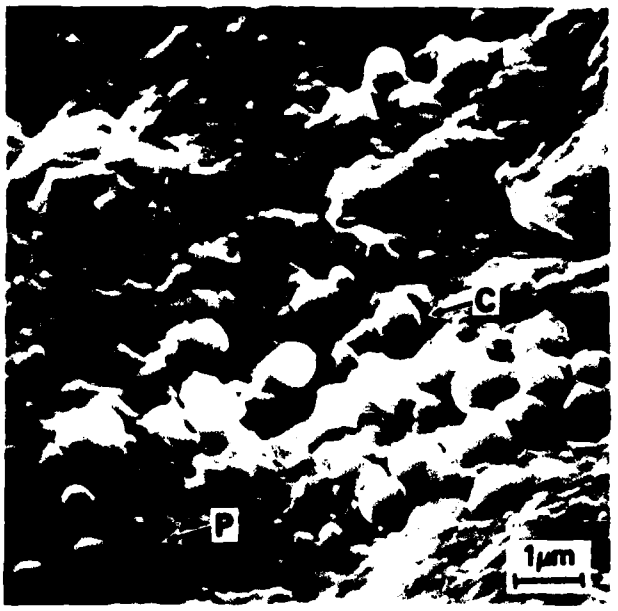

Figure 3. Spheroidal wear debris on fatigue fracture surface of MA-87, vacuum environment, ΔK = 9 MNm$^{-3/2}$. Platelet (P) with rolled up pre-sphere, spheroid (C) detached from matrix. Large arrow shows direction of crack growth.

Figure 4. Fatigue fracture surface of MA-87 cycled at $\Delta K = 8\ MNm^{-3/2}$ in air, showing heavily oxidized striations. Large arrow shows direction of crack growth; small arrow denotes typical oxide particle.

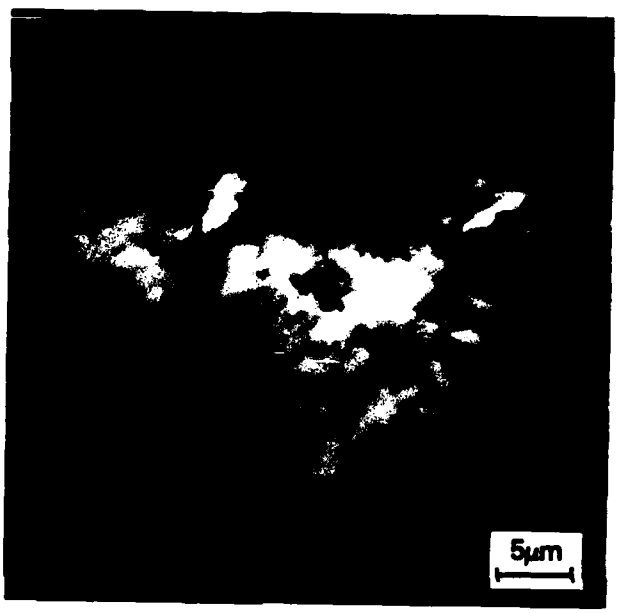

Figure 5. Oxide debris extruded from crack flank in MA-87 cycled in air, $\Delta K \simeq 10$ MNm$^{-3/2}$.

Accepted by Experimental Mechanics

CRACK TIP STRESSES AS COMPUTED FROM STRAINS DETERMINED BY STEREOIMAGING

by

D. L. Davidson*, D. R. Williams† and J. E. Buckingham*

ABSTRACT

Measurements of the three in-plane elements of the strain tensor near a crack tip have been combined with the material constitutive behavior to compute the three in-plane elements of the stress tensor and the mean stress. The method is illustrated with fatigue crack plasticity results for 7075-T6 aluminum alloy.

INTRODUCTION

One of the reasons a crack presents a threat to an engineering structure is because the nominal (design) stress to which the body is subjected is raised at the crack tip. This local stress field is in turn the driving force for crack extension. Thus, a large amount of effort has been expended over a long period of time to determine the magnitude and extent of this stress concentration. The region of elevated stress at a crack tip is very small and varies rapidly, making experimental determination of its magnitude a difficult task. It is not surprising, therefore, that most of the effort has been theoretical and computational. Fatigue cracks present special problems because of the necessity of knowing the constitutive

---

*Institute Scientist and Research Analyst at Southwest Research Institute, San Antonio, Texas 78284.

†Currently at Department of Materials Science, Northwestern University, Evanston, Illinois; previously at Southwest Research Institute.

behavior of materials subjected to cyclic loading; therefore, most of the analytical effort has gone into monotonically loaded cracks. Thus, it is understandable that fatigue crack tip stress remains a poorly quantified parameter. This paper presents a method for computing stresses in the near field of a fatigue crack from experimentally determined strains.

EXPERIMENTAL DETAILS

Single edge notched specimens of 7075-T6 aluminum alloy having a gauge section of 20 mm x 3 mm thick were pin loaded to obtain crack tip stress intensities of $6 < \Delta K < 11$ MN/m$^{3/2}$ at a frequency of 1 Hz in a vacuum of 1.3 mPa. The direction of crack growth was perpendicular to the rolling direction, and crack lengths $5 < \ell < 10$ mm were investigated.

DETERMINATION OF STRAINS

Visualization and measurement of crack tip displacements with high spatial resolution are possible using the stereoimaging technique.[1] This technique employs the ability of the eye-brain system to detect differences between two views of an object by constructing a three-dimensional image of the object. For crack tips, it is only necessary to obtain photographs in two loading states in order to image the displacements which occurred during the loading increment. The displacements imaged are in the plane of the photograph and along the eye axis. These displacements can be quantified by using the techniques of photogrammetry. The measured displacements then may be used to calculate three elements of the symmetric in-plane strain tensor.[2] Very high spatial resolution around

the crack tip can be obtained by using a special cyclic loading stage incorporated into the specimen chamber of a scanning electron microscope.[3] In this manner, the high resolution and depth of field characteristics of the SEM are utilized. Strains of up to nearly 100% have been measured, within 1 μm of the crack tip using the SEM fatigue stage and stereoimaging technique. For this purpose, photographs at magnifications up to about 10,000X have been made, although such high magnification is not normally usable because of the limited area covered. A pair of typical crack tip photographs is shown in Figure 1. This pair of photographs was used to determine the displacements shown in Figure 2. The asymmetry of displacements shown in this figure is typical of fatigue cracks grown at near-threshold stress intensities, and it is believed to be due to the propensity of metals to deform in shear. At higher stress intensities, greater symmetry of displacements is observed. As shown in Figure 1a, the crack is closed at minimum load; crack opening for this case has been found to occur at approximately 0.4 of maximum load. At full load, crack opening is a mix of Mode I and Mode II, as may be deduced from displacements behind the crack tip in Figure 2.

From the x and y displacements of Figure 2, the coordinate strain increments* $\Delta\lambda_{xx}$ and $\Delta\lambda_{yy}$, and the shear strain increment $\Delta\gamma_{xy}$ may be computed.[2] The principal strain increments $\Delta\lambda_1$ and $\Delta\lambda_2$ and the maximum shear strain increment $\Delta\gamma_{max}$ may then be computed from the coordinate

---

*The strains computed are referred to as strain increments because they refer to the strain change between two loading states. For a fatigue crack tip, the strain at minimum load is usually not at zero strain, as referenced to the uncracked state.

strains by the appropriate transformation operations (Mohr's circle). These in-plane strains are all that may be determined, since no method has yet been devised to measure the z-axis displacement gradients. Typical distributions of the principal strain increments are shown in Figures 3a, b, and c. These were derived from the displacements of Figure 2. A detailed account of computation of strains has already been given.[2]

COMPUTATION OF STRESSES

The procedure for computing stresses from strains was derived by Lubahn and Felgar.[4] Their procedure was developed to use strains as measured by electrical resistance strain gage rosettes placed on the surface. The use of their procedure with strains determined from stereoimaging is, therefore, a completely analogous situation.

The surface of any specimen is, by definition, in a state of plane stress, which means that no constraint exists normal to the surface. Thus, a limitation of the stereoimaging technique is that only surface stresses may be computed.

The strains determined by stereoimaging are total strains, and, since they are the result of changes between two loading states, they are actually total strain increments; thus, $\Delta\lambda_i$, the measured strain increment, is in general

$$\Delta\lambda_i = \Delta\varepsilon_i + \Delta e_i \qquad (1)$$

where $\Delta\varepsilon_i$ and Δe_i are the plastic and elastic strain increments, respectively. With several assumptions, Appendix A, it is possible to separate the elastic and plastic strain increments and to compute the principal stress increments

$\Delta\sigma_1$, $\Delta\sigma_2$ and $\Delta\tau_{max}$, and the coordinate stress increments $\Delta\sigma_{xx}$, $\Delta\sigma_{yy}$ and $\Delta\tau_{xy}$. A constitutive equation is required to make the strain-to-stress transformation, and it has been necessary to assume that the principal stresses have the same direction as the principal strains over one-half of the loading cycle.

The computational procedure was devised by Lubahn and Felgar for nonreverse-loaded bodies, but its use for cyclic loading is believed to be appropriate for several reasons: (1) the strain-to-stress transformation is made only for each half cycle; therefore, the increment of straining is for only the tensile or compressive loading segment of the cycle; and (2) the assumptions of plasticity theory are equally valid in tension and compression.

The strain increment data of Figure 3 have been converted to incremental stress using the procedure given in Appendix A, incorporating the mechanical properties values in Table I. Maximum principal stress increment ($\Delta\sigma_1$), minimum principal stress increment ($\Delta\sigma_2$) and the maximum shear stress increment ($\Delta\tau_{max}$) distributions near the fatigue crack tip are shown in Figures 4a, b, and c.

The mean stress is also easily computed from $\Delta\sigma_1$ and $\Delta\sigma_2$, and the distribution of this term is shown in Figure 5. Mean stresses are often considered to be useful in understanding the effects of environment and stress state on crack tip plasticity.

The conversion of the principal stresses $\Delta\sigma_i$ back into coordinate stresses in the fixed spatial x-y coordinate system is easily accomplished by using a Mohr's circle construction. Coordinate stresses are required in

cases where a sequence of loading and unloading is followed step by step, in that the summation of stresses may be done only in the fixed coordinate system.

TABLE I

Mechanical Properties
7075-T6

Tensile Proportional Limit Stress	448 MPa
Tensile 0.2% Offset Yield Stress	508 MPa
Stress-Strain Curve in Tension	$\Delta\sigma(\text{MPa}) = 7.1\text{x}10^4\ \Delta\lambda \quad 0 < \Delta\lambda < .0166$
	$\Delta\sigma(\text{MPa}) = 1620(\frac{\Delta\varepsilon}{2})^{.062} \quad .0166 \leq \Delta\varepsilon < 1$

DISCUSSION

The procedure for computing stresses from strains outlined herein is complex only to the degree expressed by Equations (A5) and (A6). The quadratic form of these equations does pose some problems with convergence, but these have been circumvented by anticipating the conditions for which convergence had been achieved. A procedure was formulated to force convergence, and it was successful for the vast majority of cases tested. Most of the cases converged within 3 to 5 iterations through the procedure given in Appendix A.

The significant opportunities for error in the stress computation procedure are related to the assumptions made. Of these, perhaps the most questionnable assumption is that of the deformation theory of plasticity, Equation (A2), which is valid only for proportional loading. Limited effort to examine this issue indicates that strain actually does increase in a reasonably proportional way for many of the points within the plastic zone on the loading portion of the cycle.

Another possible source of error is the constitutive equation, in this case the tensile stress-strain curve obtained on the loading portion of the cycle after a schedule of increasing strain-increment, reversed cyclic loading. The assumption is that this curve, derived from uniaxial tests, in which $\Delta\lambda$ is controlled, is applicable to the biaxial deformation of material near the crack tip. Lambda and Sidebottom[5,6] have examined cyclic hardening under changing biaxial conditions, and found that the result was essentially the same as for uniaxial cycling when compared on effective stress and strain basis. Fatigue crack movement in the growth rate region being studied (10^{-6} m/cy and below) is certainly slow enough for a small volume of material to be cycled enough times to achieve a stable $\Delta\sigma$. The other assumption related to the tensile stress-strain curve used is that the strain magnitude of the uniaxial tests is lower than the strain magnitudes experienced near the crack tip, so the measured results must be extrapolated to large strains. The cyclic stress-strain curve, that is the curve relating the saturation value of $\Delta\sigma$ to $\Delta\varepsilon$, as derived from a strain-controlled, reverse cycling uniaxial specimen, was also used for computation of the stress for comparison with the computation described in the previous paragraph. The result produced values near the crack tip which were 3.4% lower.

The validity of using these constitutive equations near a fatigue crack tip has not been confirmed, partly because there is no independent way to measure stresses near crack tips with the required resolution. However, stresses computed by the methods outlined here have been matched with those determined indirectly from using subgrains formed near fatigue crack tips in low-carbon steel as "stress gages," and the results were found to be very nearly the same.[7] Also, strains measured on a polycarbonate tensile specimen were converted to stresses using Hookes Law and matched to the measured stress. For a strain of approximately 0.01, the stress computed was within 3% of that measured.

The results presented here are interesting, from the viewpoint of crack tip mechanics. The maximum principal stress increment at the crack tip is 1490 MPa. This is 3 times the 0.2% offset stress from a uniaxial tensile test (508 MPa), and 1.7 times the cyclic yield stress (880 MPa), defined as the stress for $\Delta\varepsilon = 0.02\%$. The maximum value of mean stress (1180 MPa) occurred 10 μm ahead of the crack tip, decreasing to 1120 MPa at the crack tip.

The outer plastic zone, defined as the distance ahead of the crack tip where $\Delta\sigma_1$ exceeds 508 MPa, occurs at a distance beyond that of the strain analysis, but it is extrapolated to be 110 μm. The inner, or cyclic plastic zone, defined as the distance ahead of the crack tip where $\Delta\sigma_1$ exceeds 880 MPa, is 60 μm. These compare with the net section stress of 50 MPa which would be reached at a distance of 160 μm ahead of the crack tip (as determined by extrapolation). Note that the stress gradient within the plastic zone is much more gradual than the strain gradient, as would be expected from the low work hardening coefficient of this alloy.

Values of plastic zone size (PZS) may be computed using the equation

$$PZS = \alpha\left(\frac{K}{\sigma_i}\right)^2 \qquad (2)$$

where PZS refers to the cyclic zone when σ_i = cyclic yield stress and to the outer PZS when σ_i = tensile yield stress. This equation is an estimate made by Rice[8] for non-work hardening materials. He estimated that for plane stress $\alpha_o = 0.32$ for the outer plastic zone size ahead of the crack, and $\alpha_c = \frac{1}{4}\alpha_o$ for the cyclic plastic zone. For the plastic zone size estimates given in the previous paragraph, α_o and α_c are computed to be: $\alpha_o = .44$, $\alpha_c = .72$, with $\alpha_c = 1.6\ \alpha_o$. Estimates of PZS by Eq. (2), therefore, result in values smaller than are determined here.

SUMMARY AND CONCLUSIONS

1. A procedure for computing the three in-plane elements of the principal stress tensor from the in-plane strain tensor, as measured by stereoimaging, has been adapted from the work of Lubahn and Felgar.[4]
2. Stresses in the near-crack tip region have been computed for a fatigue crack tip in 7075-T6. The maximum and minimum principal stresses, maximum shear stress and mean stress distributions near the crack tip are illustrated, together with the principal strain distributions, which are the measured values.
3. The maximum principal stress is computed to be 3 times the yield stress and 1.7 times the cyclic yield stress. The maximum value of mean stress is found to be 10 μm ahead of the crack tip.

APPENDIX A

Calculation of the principal stress increments from the principal strain increments has been done according to the method derived by Lubahn and Felgar.[4] This appendix outlines the method and gives the assumptions used in the computation.

The following assumptions are necessary in order to make the computation:

1) $\Delta\sigma_3 = 0$; a condition of plane stress pertains

2) $\Delta\lambda_i = \Delta\varepsilon_i + \Delta e_i$ ($i = 1$ or 2 for the principal strains) (A1)

3) The deformation theory of plasticity pertains, so that, with $\Delta\sigma_3 = 0$

$$\frac{\Delta\varepsilon_1-\Delta\varepsilon_2}{\Delta\sigma_1-\Delta\sigma_2} = \frac{\Delta\varepsilon_2-\Delta\varepsilon_3}{\Delta\sigma_2} = \frac{\Delta\varepsilon_3-\Delta\varepsilon_1}{\Delta\sigma_1} \tag{A2}$$

4) During plastic deformation, plastic strain does not cause a volume change, so that

$$\Delta\varepsilon_1 + \Delta\varepsilon_2 + \Delta\varepsilon_3 = 0 \tag{A3}$$

5) The elastic stress-strain relations are:

$$\Delta e_1 = \frac{\Delta\sigma_1}{E} - \frac{\mu}{E}\Delta\sigma_2$$

$$\Delta e_2 = \frac{\Delta\sigma_2}{E} - \frac{\mu}{E}\Delta\sigma_1 \tag{A4}$$

$$\Delta e_3 = \frac{\mu}{E}(\Delta\sigma_1 + \Delta\sigma_2)$$

These equations may be combined and reduced to a quadratic equation in $\Delta\sigma_2$:

$$a\,\Delta\sigma_2^2 + b\,\Delta\sigma_2 + c = 0 \tag{A5}$$

where $a = 1-2\mu$ $\quad b = -E(2\Delta\lambda_1 + \Delta\lambda_2)$ $\quad c = -[\Delta\sigma_1^2 a + \Delta\sigma_1 b]$

so that

$$\Delta\sigma_2 = \frac{-b-\sqrt{b^2-4ac}}{2a} \tag{A6}$$

The computational procedure for calculating the principal stress increments from the principal strain increments is as follows:

1. If both $\Delta\lambda_1$ and $\Delta\lambda_2$ are less than the elastic limit strain in a tensile sample, $\Delta\sigma_1$ and $\Delta\sigma_2$ are computed from Equation (A4). For all other cases, steps 2-9 are followed.
2. Assume a value of $\Delta\sigma_1$.
3. Compute $\Delta\sigma_2$ from (A6).
4. Compute $\Delta\sigma^s_{eff} = (\Delta\sigma_1^2 - \Delta\sigma_1\Delta\sigma_2 + \Delta\sigma_2^2)^{1/2}$. (A7)
5. Compute Δe_i from (A4).
6. Compute $\Delta\varepsilon_i$ from (A1).
7. Compute $\Delta\varepsilon_{eff} = \frac{2}{\sqrt{3}}(\Delta\varepsilon_1^2 + \Delta\varepsilon_1\Delta\varepsilon_2 + \Delta\varepsilon_2^2)^{1/2}$. (A8)
8. Determine $\Delta\sigma^e_{eff}$ from the appropriate stress-strain relation for the material*. For fatigue cracks, an equation of the following form has been used:

$$\Delta\sigma^e_{eff} = K_1\left(\frac{\Delta\varepsilon_{eff}}{2}\right)^m \tag{A9}$$

---

*The cyclic stress-strain relation is normally obtained from a specimen stressed along one axis, while the fatigue crack creates a multiaxial stress state. It has been assumed that the cyclic stress-strain curve may be related to the multiaxial case through use of the effective stress and strain. This assumption has been examined by Lambda and Sidebottom[5,6] who found no reason to invalidate it.

9. Compare $\Delta\sigma^s_{eff}$ with $\Delta\sigma^e_{eff}$. If $\left|\Delta\sigma^s_{eff} - \Delta\sigma^e_{eff}\right|$ is greater than a specified tolerance, assume another value of $\Delta\sigma_1$ and return to step 2. A new value of $\Delta\sigma_1$ is determined from

$$\Delta\sigma_1' = \Delta\sigma_1 \left(\frac{\Delta\sigma^e_{eff}}{\Delta\sigma^s_{eff}}\right) \tag{A10}$$

ACKNOWLEDGEMENT

The financial support by the Office of Naval Research, Contract Number N00014-75-C-1038, Dr. Philip Clarkin, technical monitor, is gratefully acknowledged. We are pleased to acknowledge the assistance of Prof. Sol R. Bodner of the Technion who pointed out the procedure in Lubahn and Felgar giving the basic ideas repeated in Appendix A, and was helpful through other technical discussions. Dr. U. S. Lindholm of SwRI also contributed many useful points in numerous discussions.

REFERENCES

1. Davidson, D. L., "The Observation and Measurement of Displacements and Strain by Stereoimaging," Scanning Electron Microscopy/1979/II, pp. 79-86 (1979).

2. Williams, D. R., Davidson, D. L., and Lankford, J., "Fatigue-Crack-Tip Plastic Strains by the Stereoimaging Technique," Experimental Mechanics, 20, pp. 134-139 (1980).

3. Davidson, D. L. and Nagy, A., "A Low Frequency Cyclic Loading Stage for the SEM," Journal of Physics E, V. 11, pp. 207-210 (1978).

4. Lubahn, J. D. and Felgar, R. P., Plasticity and Creep of Metals, John Wiley, and Sons, Inc., New York, pp. 321-325 (1961).

5. Lambda, H. S. and Sidebottom, O. M., "Cyclic Plasticity for Nonproportional Paths: Part 1 - Cyclic Hardening Erasure of Memory, and Subsequent Strain Hardening Experiments," Trans. ASME: J. of Engineering Mater. and Tech., V. 100, pp. 96-103 (1978).

6. Lambda, H. S. and Sidebottom, O. M., "Cyclic Plasticity for Nonproportional Paths: Part 2 - Comparison with Predictions of Three Incremental Plasticity Models," Trans. ASME: J. of Engineering Mater. and Tech., V. 100, pp. 104-109 (1978).

7. Davidson, D. L. and Lankford, J., "The Effect of Water Vapor on Fatigue Crack Tip Stress and Strain Range Distribution and the Energy Required for Crack Propagation in Low-Carbon Steel," International Journal of Fracture, V. 17, No. 3, pp. 257-275 (1981).

8. Rice, J. R., "Mechanics of Crack Tip Deformation and Extension by Fatigue," ASTM STP 415, Am. Soc. Test. and Mater., Philadelphia, pp. 247-309 (1967).

SYMBOLS

Δ	=	increment of a quantity
e_i	=	elastic strain (i = x, y, z or 1, 2, 3)
ε_i	=	plastic strain
λ_i	=	total strain
ε_{eff}	=	effective strain, defined by Eq. (A8)
σ_i	=	stress
σ_{eff}	=	effective stress, defined by Eq. (A7)
E	=	Young's modulus
μ	=	Poisson's ratio

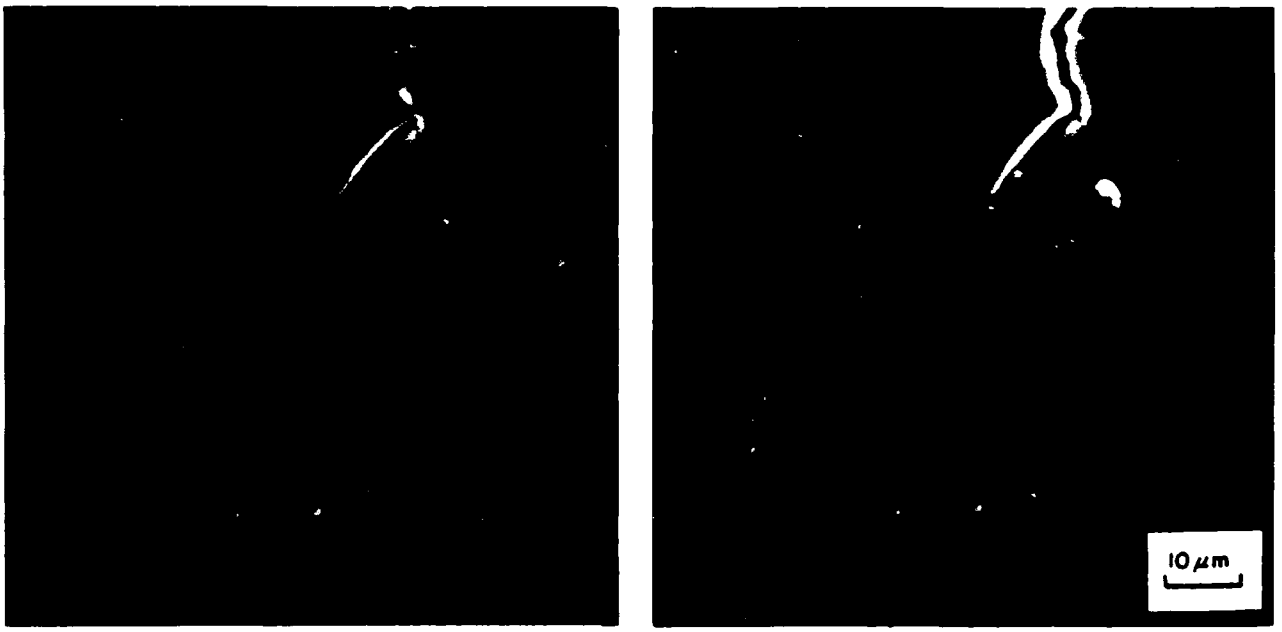

(a) Minimum load level, K = 2.7 $MN/m^{3/2}$ (b) Maximum load level, K = 10.7 $MN/m^{3/2}$

Figure 1. Photographs of the crack tip for which the analyses in this paper are made. 7075-T6 aluminum alloy grown in vacuum at $\Delta K = 8\ MN/m^{3/2}$, R = 0.25.

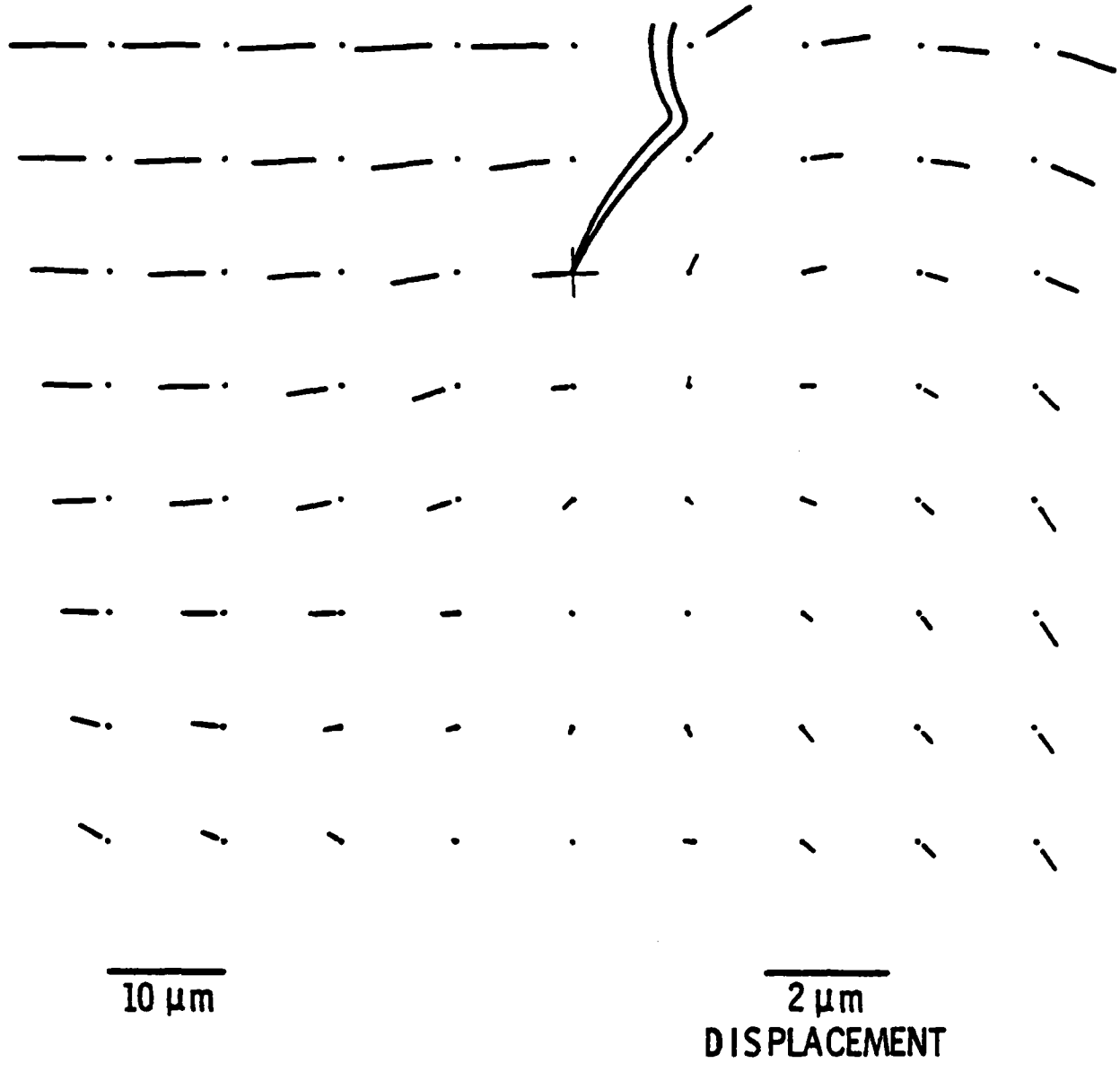

(a) Coarse grid

Figure 2. Displacements measured from the photographs shown in Figure 1. Notice that the length of the displacements is magnified relative to the spatial distances shown. The dot marks the undeformed location and the end of the line displacement due to the loading increment.

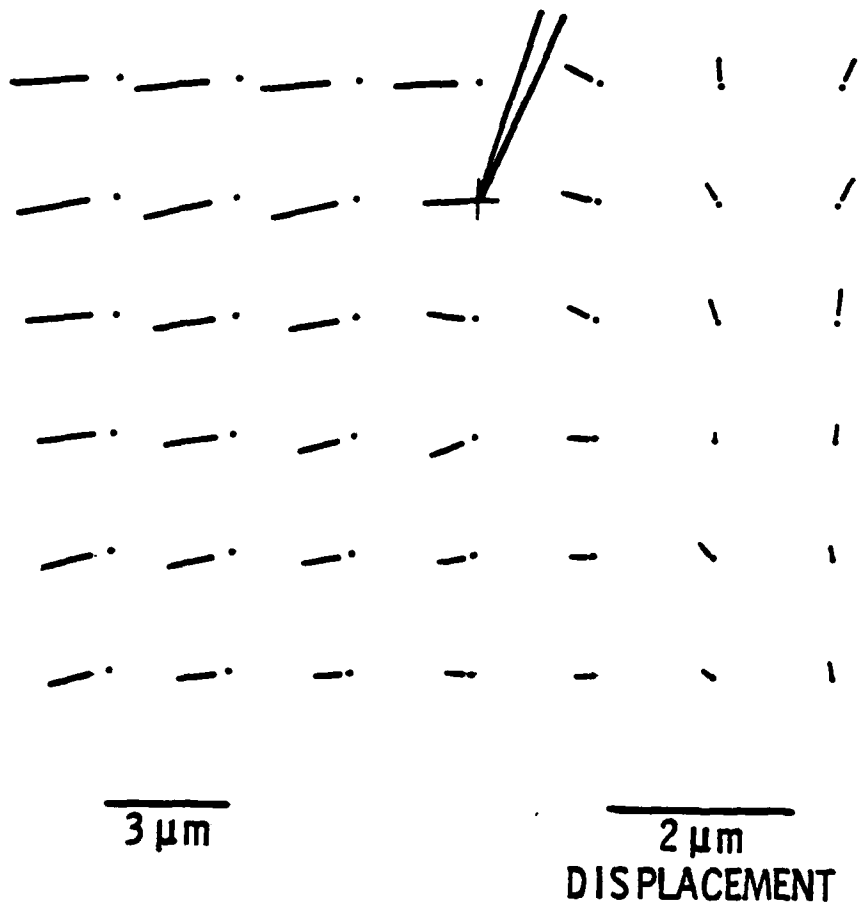

(b) Fine grid

Figure 2 (continued). Displacements measured from the photographs shown in Figure 1. Notice that the length of the displacements is magnified relative to the spatial distances shown. The dot marks the undeformed location and the end of the line displacement due to the loading increment.

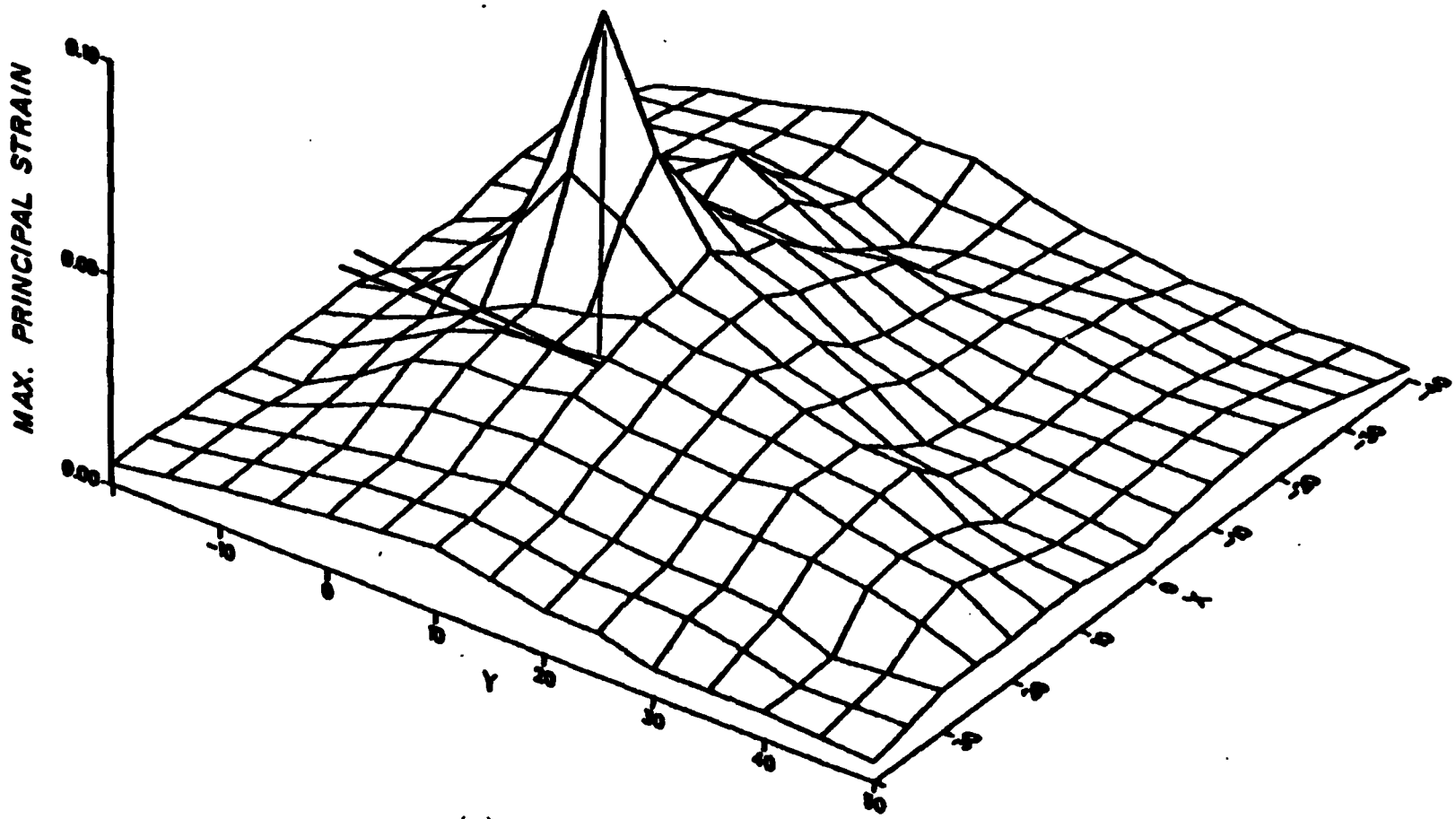

(a) Maximum principal strain increment

Figure 3. Maximum values of the strains derived from the displacements shown in Figure 2. Distances along the x and y axes are in micrometers. The crack is shown schematically on the plane of zero strain.

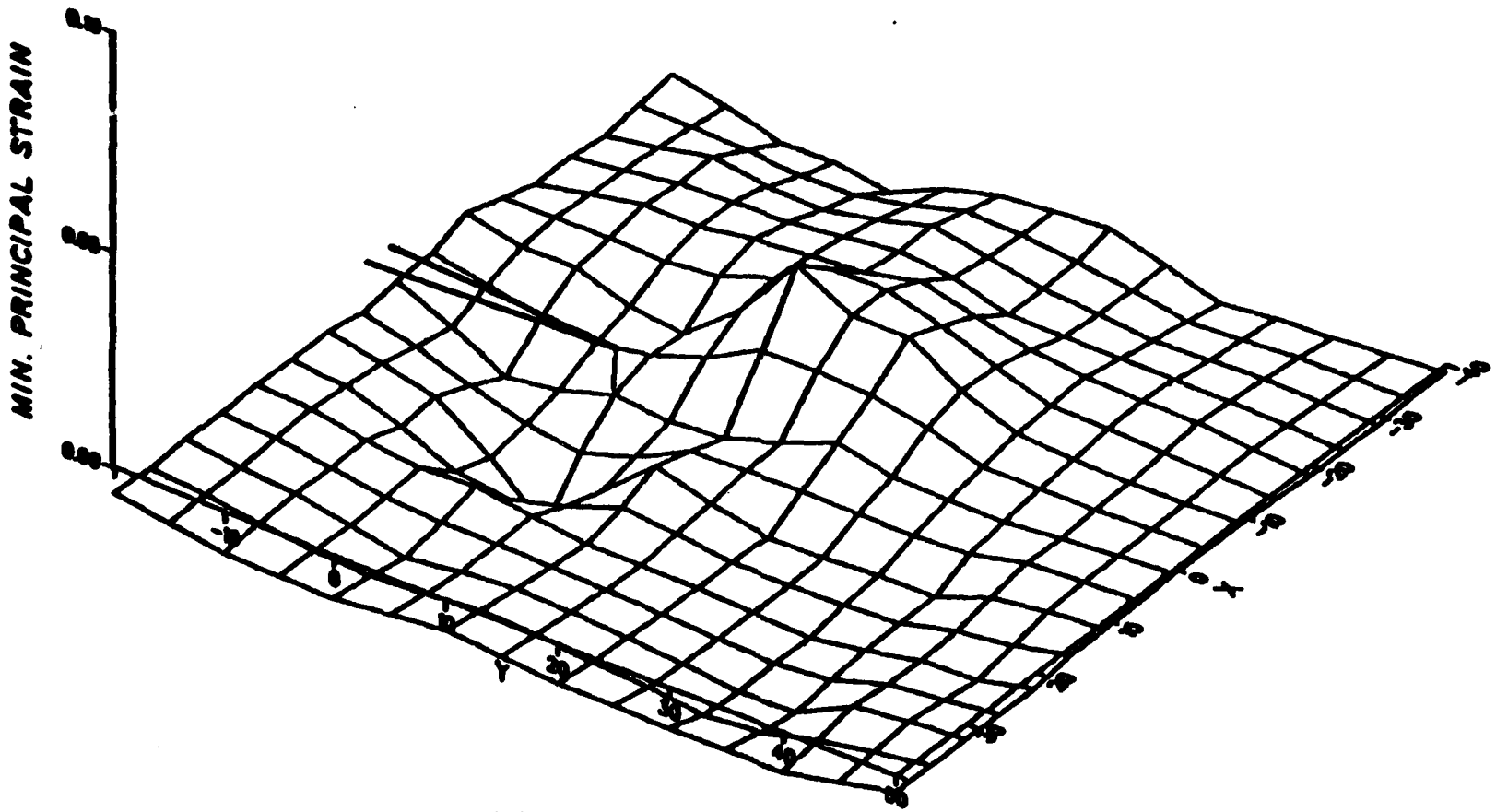

(b) Minimum principal strain increment

Figure 3 (continued). Maximum values of the strains derived from the displacements shown in Figure 2. Distances along the x and y axes are in micrometers. The crack is shown schematically on the plane of zero strain.

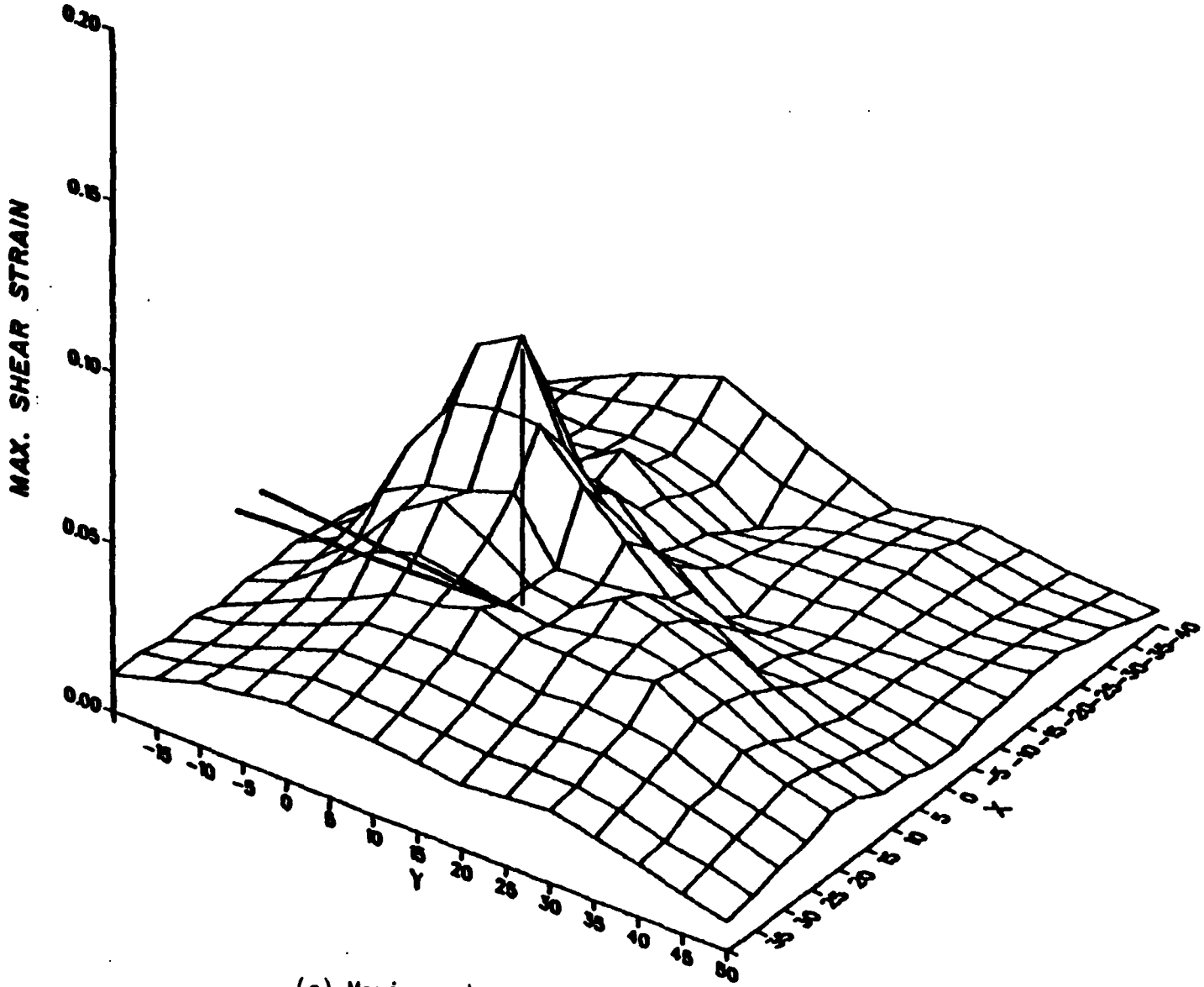

(c) Maximum shear strain increment

Figure 3 (continued). Maximum values of the strains derived from the displacements shown in Figure 2. Distances along the x and y axes are in micrometers. The crack is shown schematically on the plane of zero strain.

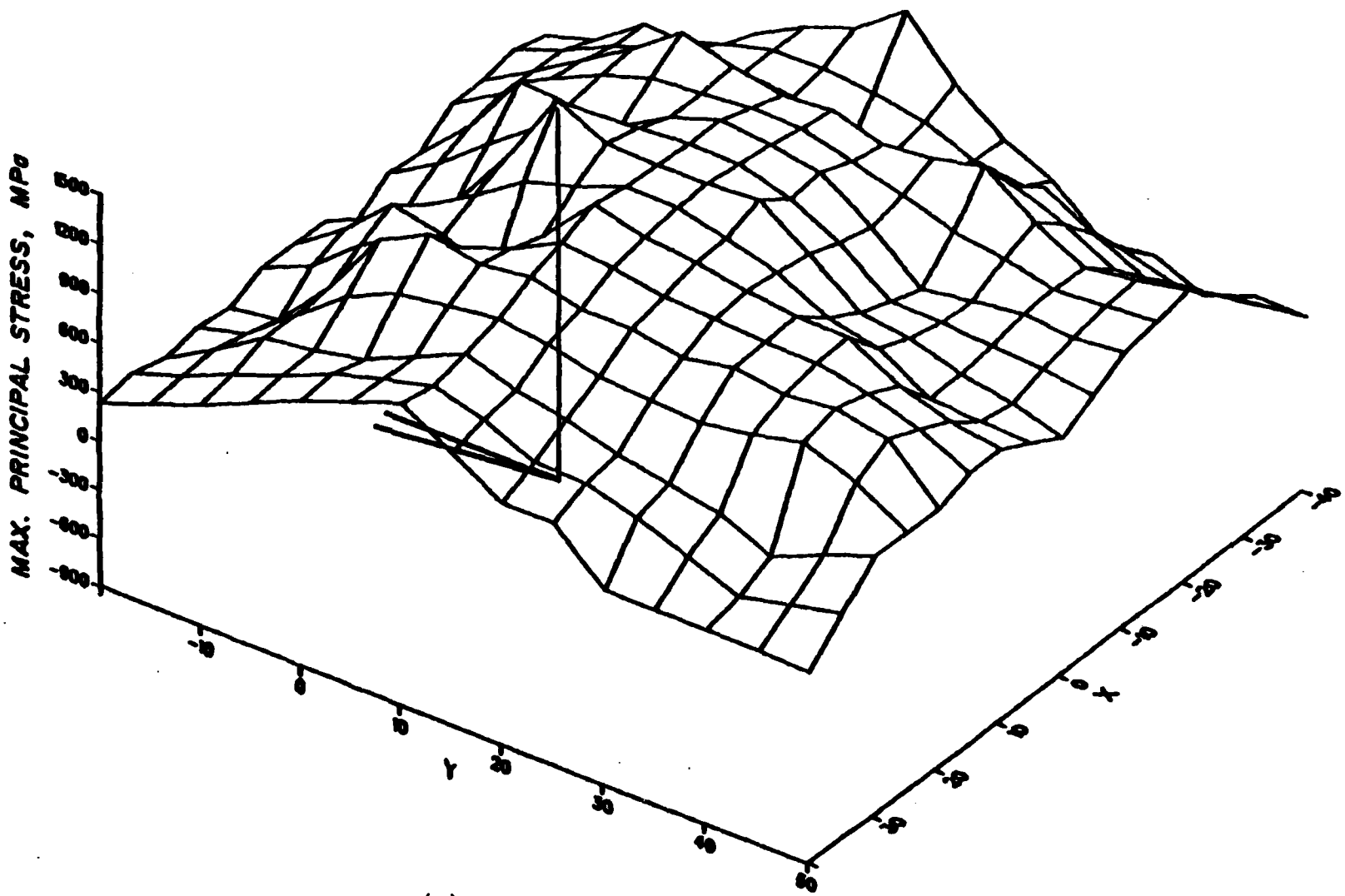

(a) Maximum principal stress increment

Figure 4. Maximum values of the stresses computed from the strains of Figure 3 in MPa. Distances along the x and y axes are in micrometers. The crack is shown schematically on the plane of zero stress.

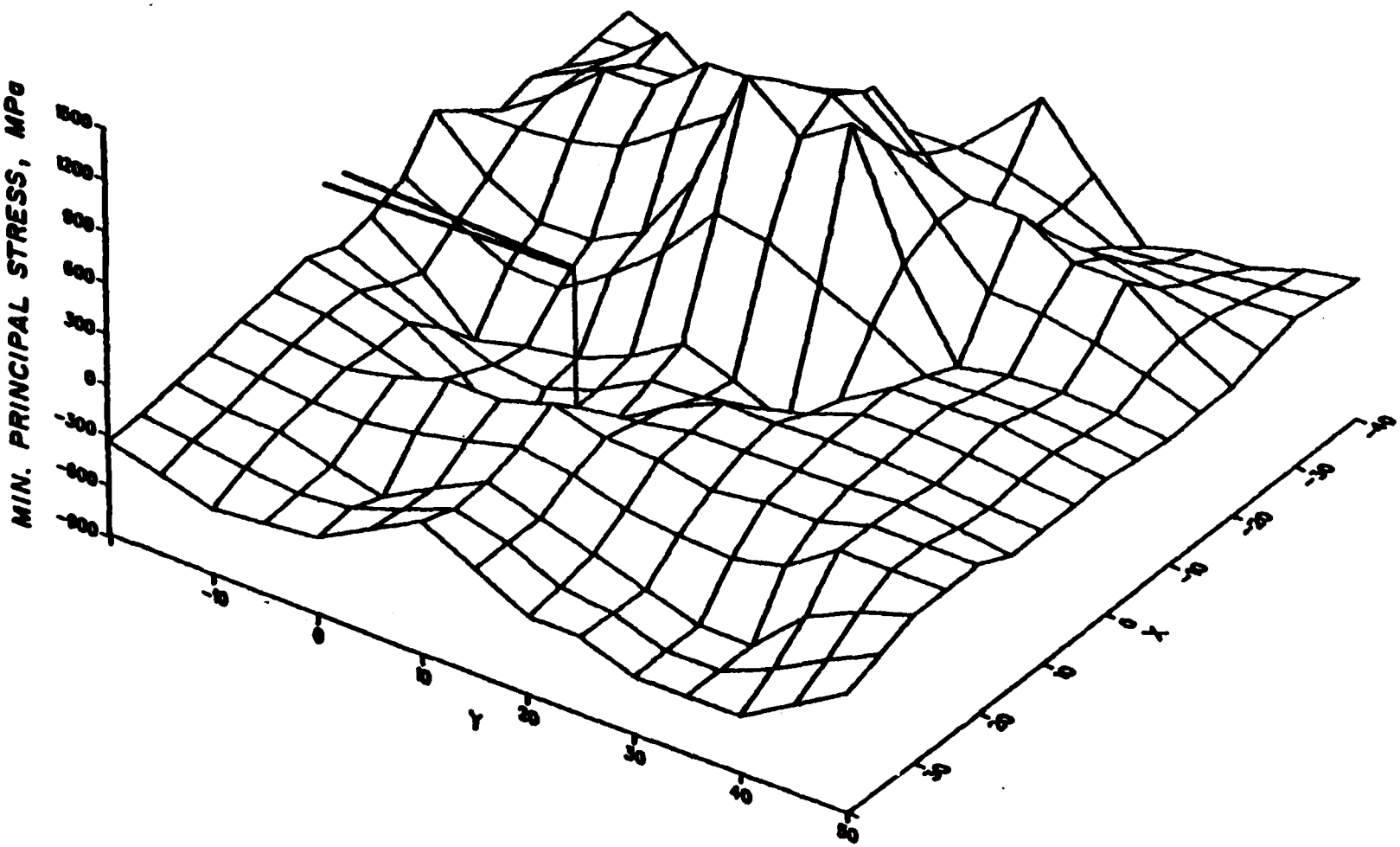

(b) Minimum principal stress increment

Figure 4 (continued). Maximum values of the stresses computed from the strains of Figure 3 in MPa. Distances along the x and y axes are in micrometers. The crack is shown schematically on the plane of zero stress.

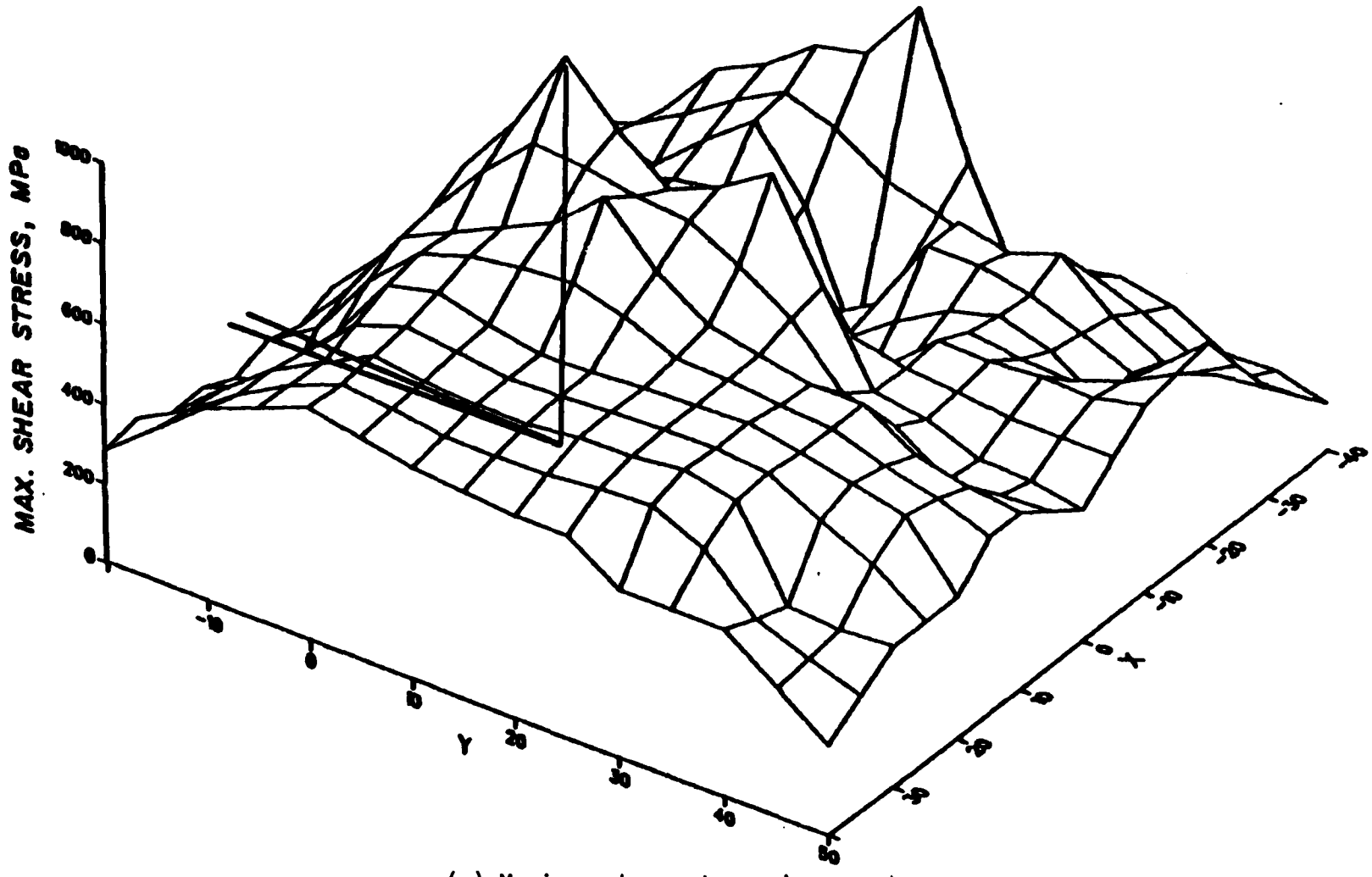

(c) Maximum shear stress increment

Figure 4 (continued). Maximum values of the stresses computed from the strains of Figure 3 in MPa. Distances along the x and y axes are in micrometers. The crack is shown schematically on the plane of zero stress.

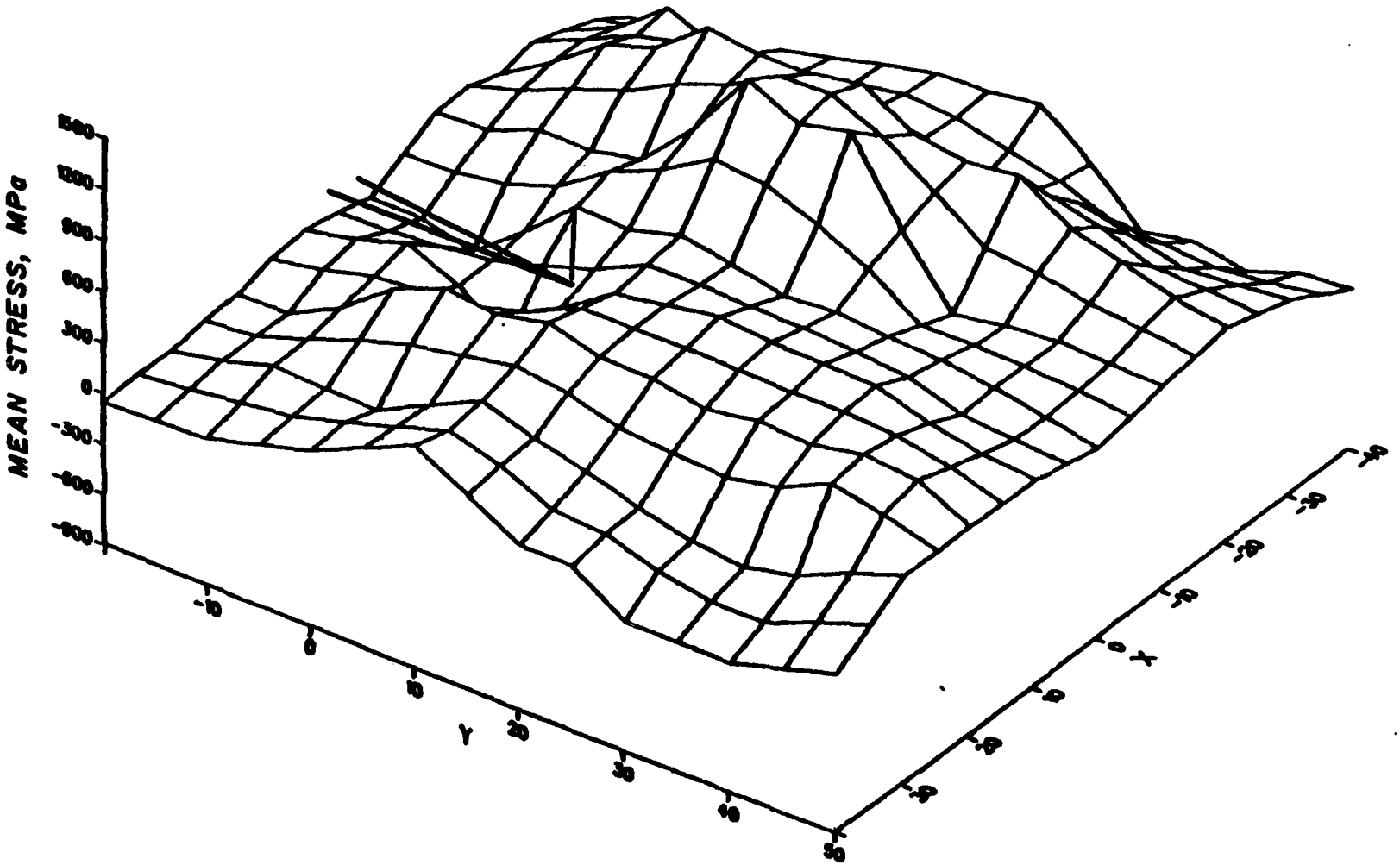

Figure 5. Mean stress increment $\frac{1}{2}(\Delta\sigma_1 + \Delta\sigma_2)$ in MPa, derived from the values shown in Figure 4. Distances along the x and y axes are in micrometers.